CHIN. PHYS. LETT. Vol. 38, No. 5 (2021) 057305

Interfacial Charge Transfer Induced Electronic Property Tuning of MoS_2 by Molecular Functionalization

Si-Han Zhou(周思含), Chun-Wei Zhou(周春伟), Xiang-Dong Yang(杨向东), Yang Li(李阳), Jian-Qiang Zhong(钟建强)*, and Hong-Ying Mao(毛宏颖)*

Department of Physics, Hangzhou Normal University, Hangzhou 311121, China

(Received 25 November 2020; accepted 9 March 2021; published online 2 May 2021)

The modulation of electrical properties of MoS_2 has attracted extensive research interest because of its potential applications in electronic and optoelectronic devices. Herein, interfacial charge transfer induced electronic property tuning of MoS_2 are investigated by *in situ* ultraviolet photoelectron spectroscopy and x-ray photoelectron spectroscopy measurements. A downward band-bending of MoS_2-related electronic states along with the decreasing work function, which are induced by the electron transfer from Cs overlayers to MoS_2, is observed after the functionalization of MoS_2 with Cs, leading to n-type doping. Meanwhile, when MoS_2 is modified with 2,3,5,6-tetrafluoro-7,7,8,8-tetracyanoquinodimethane (F_4-TCNQ), an upward band-bending of MoS_2-related electronic states along with the increasing work function is observed at the interfaces. This is attributed to the electron depletion within MoS_2 due to the strong electron withdrawing property of F_4-TCNQ, indicating p-type doping of MoS_2. Our findings reveal that surface transfer doping is an effective approach for electronic property tuning of MoS_2 and paves the way to optimize its performance in electronic and optoelectronic devices.

DOI: 10.1088/0256-307X/38/5/057305

Since the discovery of their novel and intriguing properties, two-dimensional (2D) layered transition metal dichalcogenides (TMDs) have attracted extensive attention because of their potential applications in optoelectronic devices, field effect transistors (FETs), and electrocatalysts,[1−11] among which MoS_2 is one of the most promising candidates for both fundamental investigations and technological applications. The MoS_2 crystal consists of a hexagonally packed layer of Mo atoms, which is sandwiched between two layers of S atoms.[12] Because of the strong intra-layer interaction within molecular layers and the weak inter-layer interaction between molecular layers, single-layer, as well as few-layer, MoS_2 can be isolated by mechanical, liquid phase and intercalation-assisted exfoliations.[13−15] Moreover, bottom-up approaches for controlled synthesis of MoS_2 have also been realized by chemical vapor deposition.[16−18]

Considering the applications of MoS_2 in electronic and optoelectronic devices, the modulation of its electronic band structure is of critical importance.[12] Dimension tuning along the z direction is an effective approach to modulate the electronic band structure of MoS_2. Bulk MoS_2 is of semiconductor with an indirect band gap of 1.2 eV. By thinning bulk MoS_2 to an atomic monolayer, a crossover from indirect to direct band gap can be achieved. Meanwhile, the band gap increases to 1.8 eV due to quantum confinement effects.[19−21] Intercalation tuning is another promising approach that has been developed in recent years. The most commonly used intercalants include alkali metal and 3d transition metal atoms.[22] The electronic properties of MoS_2 are effectively tuned because of the charge transfer between the intercalants and chalcogenide layers. Finally, the electronic modulation of MoS_2 can also be realized by heterojunction engineering, especially in controlling its carrier density without sacrificing the carrier mobility.[23−25] Tunable photoluminescence of monolayer MoS_2 has been achieved by choosing n-type or p-type dopants, and the enhanced photoluminescence was attributed to the switch between exciton photoluminescence and trion photoluminescence, which depends on the carrier density in inmonolayer MoS_2.[23] Surface functionalization is a promising approach for electronic property tuning of MoS_2. Electron transfer from alkali metals to a single crystal MoS_2 has been observed along with supra-valence electrons in oxidation reactions.[26−28] Charge carrier modulation within MoS_2 has been realized via molecular decoration with 2,3,5,6-tetrafluoro-7,7,8,8-tetracyanoquinodimethane (F_4-TCNQ), which leads to enhanced device performance for MoS_2-based optoelectronic devices and gas sensors.[25,29,30] However, most of these studies were focused on electrical characterization or photoluminescence measurements. A comprehensive understanding from the point view

Supported by the National Natural Science Foundation of China (Grant No. 22002031), the Natural Science Foundation of Zhejiang Province (Grant No. LY18F010019), and the Innovation Project in Hangzhou for Returned Scholar.
*Corresponding authors. Email: zhong@hznu.edu.cn; phymaohy@hznu.edu.cn
© 2021 Chinese Physical Society and IOP Publishing Ltd

of energy level alignments at the interface between surface functionalization overlayers and MoS_2 is still highly desired.

In this Letter, interfacial charge transfer induced electronic property tuning of MoS_2 is realized using Cs and F_4-TCNQ, respectively. As revealed by *in situ* x-ray photoelectron spectroscopy (XPS) and ultraviolet photoelectron spectroscopy (UPS), the Mo $3d_{5/2}$ and S $2p_{3/2}$ core levels shift to high binding energy part when MoS_2 is functionalized with Cs. Meanwhile, its work function (WF) decreases from 4.50 eV to 2.72 eV as compared to pristine MoS_2. As a result, the Fermi level of MoS_2 shifts upward to its conduction band minimum (CBM) because of the electron transfer from Cs to MoS_2 at the interface. In the case of F_4-TCNQ modified MoS_2, interfacial electron transfer takes place under the opposite direction. Because of the strong electron withdrawing property, spontaneous electron transfer from MoS_2 to F_4-TCNQ occurs, which leads to p-type doping of MoS_2. This is corroborated by an upward band-bending of MoS_2-related electronic states along with the increasing work function.

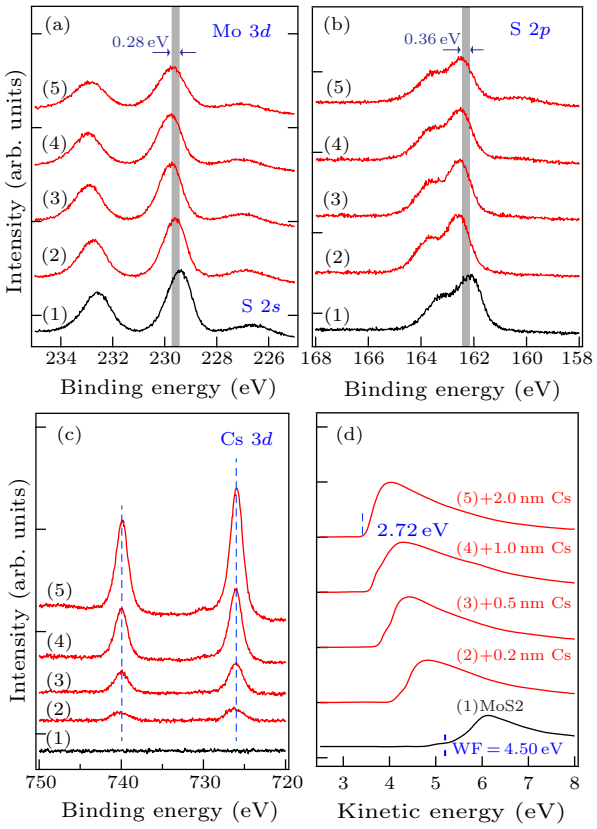

Fig. 1. XPS core level spectra of (a) Mo 3*d*, (b) S 2*p*, (c) Cs 3*d*, and (d) UPS spectra at the low kinetic energy region with the increasing coverage of Cs on bulk MoS_2.

Using a multifunctional ultrahigh vacuum (UHV) VT-SPM system (Omicron Instruments for Surface Science), *in situ* UPS and XPS measurements were performed to investigate n- and p-type doping of MoS_2 by molecular functionalization. He I (21.2 eV) was used as the excitation source when UPS measurements were carried out. The sample WF was determined by the linear extrapolation at the low kinetic energy region of UPS spectra and a −5 V sample bias was applied for WF measurements. During UPS measurements, the base pressure in the analysis chamber was better than $\sim 3 \times 10^{-8}$ mbar. XPS measurements were carried out with an Al K_α source (1486.6 eV). A sputtered clean gold sample was used to calibrate the binding energy for all XPS spectra. The bulk MoS_2 (HF-Kejing) was peeled with scotch tape to reveal a fresh surface before annealing in the preparation chamber at 200℃ overnight helpful to remove surface adsorbates and other contaminants. The morphology of bulk MoS_2 (shown in Fig. S1 in the Supplementary Material) was measured by an atomic force microscope (AFM, Being Nano-Instruments CSPM 5500). A commercial SAES Cs getter source was used for deposition of Cs on MoS_2 and the deposition rate was calibrated by a quartz crystal microbalance (QCM). After thoroughly degassing, perylenetetracarboxylic dianhydride (PTCDA) and F_4-TCNQ (Sigma-Aldrich) were deposited onto MoS_2 by thermal deposition methods using a Knudsen cell when the base pressure in the growth chamber was better than 1×10^{-8} mbar. The nominal thicknesses of PTCDA and F_4-TCNQ were monitored by the QCM and confirmed by the attenuation of Mo 3*d* XPS core levels after the deposition of organic molecules.

The n-type doping of MoS_2 has been investigated using *in situ* UPS and XPS measurements. Figures 1(a)–1(c) show the XPS core level spectra of Mo 3*d*, S 2*p*, and Cs 3*d* with the increasing coverage of Cs on bulk MoS_2. For pristine MoS_2, the Mo $3d_{5/2}$ peak locates at 229.38 eV, and the full width at half maximum (FWHM) is 1.18 eV. Upon the functionalization of MoS_2 with Cs, the binding energy of the Mo $3d_{5/2}$ core level increases gradually. As shown in Fig. 1(a), when the thickness of Cs increases to 2.0 nm, the binding energy of the Mo $3d_{5/2}$ peak increases by 0.28 eV to 229.66 eV. Consistent with Mo $3d_{5/2}$ core level, the binding energy of the S $2p_{3/2}$ peak increases from 162.18 eV to 162.54 eV, corresponding to a 0.36 eV shift to high binding energy part. Meanwhile, the FWHMs of Mo $3d_{5/2}$ and S $2p_{3/2}$ core level peaks do not change after Cs functionalization, indicating that it is the doping effect rather than chemical reaction that is responsible for the downward band-bending in MoS_2. Although the binding energy of Cs 3*d* core level does not change [Fig. 1(c)], there is a significant shift of the secondary electron cut-off in the low kinetic energy region upon the deposition of Cs onto MoS_2. The WF for pristine MoS_2 is 4.50 eV, and it

decreases significantly to 2.72 eV when the nominal thickness of Cs reaches 2.0 nm. The low WF of Cs leads to the spontaneous electron transfer from Cs to MoS_2 upon contact. Consequently, the Fermi level of MoS_2 shifts upward toward its CBM, leading to the downward band-bending in MoS_2. The observed large vacuum level shift (WF decrease) of 1.78 eV derives from the convolution of downward band-bending (0.28 eV) in MoS_2 and the interfacial dipole formed at the Cs/MoS_2 interface, as plotted in Fig. S2(a). It is worth noting that the decreasing WF, together with the downward band-bending Mo 3*d* and S 2*p*, is more obvious in the interface region when the coverage of Cs is 0.2 nm, and it saturates quickly when the coverage of Cs increases to 1.0 nm. This indicates that such an electron transfer from Cs to MoS_2 is more pronounced within the submonolayer coverage of surface functionalization overlayers. Finally, we need to mention that the binding energy of Cs 3*d* should shift toward high binding energy part with the increasing coverage of Cs since electron transfer from Cs to MoS_2 occurs upon the formation of Cs/MoS_2 interface. Although these binding energy shifts of dopants are not observed in the present study, a similar phenomenon is observed for surface transfer hole doping of epitaxial graphene by MoO_3 and more investigation should be carried out in future studies.[31]

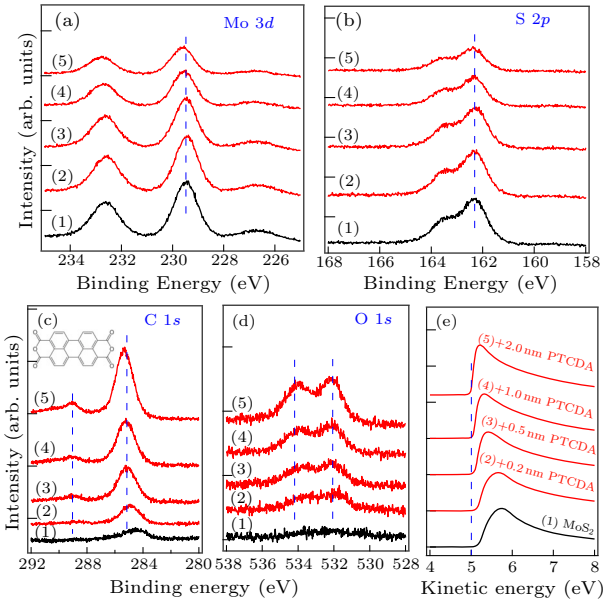

Fig. 2. XPS core level spectra of (a) Mo 3*d*, (b) S 2*p*, (c) C 1*s*, (d) O 1*s*, and (e) UPS spectra at the low kinetic energy region with the increasing coverage of PTCDA on bulk MoS_2. The inset of Fig. 2(c) shows the molecular structure of PTCDA.

The charge transfer at the interface between MoS_2 and dopants is of great importance in determining the doping efficiency. As we have discussed above, the low WF of Cs leads to the electron transfer from Cs to MoS_2, which results in the n-type doping of MoS_2. A commonly used molecule in organic optoelectronic devices, PTCDA has been chosen to investigate the interfacial charge transfer induced doping effect in MoS_2. Unlike the interface between Cs and MoS_2 where interfacial charge transfer is facilitated due to low WF of Cs, the Fermi level of MoS_2 locates in the band gap of PTCDA, which could inhibit the charge transfer after the formation of the PTCDA/MoS_2 interface.[32] As presented in Figs. 2(a) and 2(b), the binding energies of Mo $3d_{5/2}$ and S $2p_{3/2}$ peaks do not change after the modification of MoS_2 with PTCDA at the increasing coverage from 0.2 nm to 2.0 nm. It is generally believed that n-type doping leads to a downward band-bending in MoS_2, whereas p-type doping results in an upward band-bending in MoS_2. Since there are no binding energy shifts for both Mo $3d_{5/2}$ and S $2p_{3/2}$ core levels after the functionalization of MoS_2 with PTCDA overlayers, we conclude that no doping effect occurs in PTCDA/MoS_2 in view of the diagram of interfacial energy levels. Moreover, XPS results also show the unchanged C 1*s* and O 1*s* core levels [Figs. 2(c) and 2(d)] along with the unchanged WF [Fig. 2(e)]. There are two peaks for C 1*s* core level in PTCDA/MoS_2, as shown in Fig. 2(c), the main component at 285.28 eV is attributed to carbon atoms from the perylene core, and the weak component at 289.08 eV derives from carbon atoms from the carbonyl groups.[33–35] In the case of O 1*s* core level shown in Fig. 2(d), two peaks at 532.08 eV and 534.04 eV are attributed to anhydride and carboxylic oxygen atoms, respectively. Consistent with Mo $3d_{5/2}$ or S $2p_{3/2}$ core levels, no binding energy shifts are observed for both C 1*s* and O 1*s* core levels. In addition, the WF for PTCDA modified MoS_2 [Fig. 2(e)] is 4.46 eV, which is nearly the same as the WF of pristine MoS_2. Consequently, the Fermi level of MoS_2 locates between the highest occupied molecular orbital (HOMO) and lowest unoccupied molecular orbital (LUMO) of PTCDA. As a result, the charge transfer at the interface between PTCDA and MoS_2 is energetically unfavorable, and hence no doping effect is observed.

In the case of chemical vapor deposition grown MoS_2 films and mechanical exfoliated MoS_2 flakes, unintentional electron doping is usually observed because of the gap states below the conduction band edge, which are introduced by the sulfur vacancies. This is also confirmed by our UPS results. As shown in Fig. S3, the edge of the valence band maximum (VBM) of bulk MoS_2 is located at 1.12 eV below the Fermi level. Considering that the band gap of bulk MoS_2 is 1.2 eV, the Fermi level locates just 0.08 eV below the edge of CBM, indicating the electron doping of pristine MoS_2. To deplete residual electrons from sulfur vacancies, surface functionalization of MoS_2 by

organic molecules with strong electron withdrawing property opens up a pathway for such modulations. The electron depletion or p-type doping of MoS_2 via F_4-TCNQ overlayers is investigated by *in situ* UPS and XPS measurements. Due to the strong electron withdrawing property of F_4-TCNQ, electron transfer from MoS_2 to F_4-TCNQ takes place after the formation of F_4-TCNQ/MoS_2 interfaces, where the Fermi level of MoS_2 moves downward to its VBM, leading to the upward band-bending in MoS_2. This upward band-bending at the interface is confirmed by our XPS results.

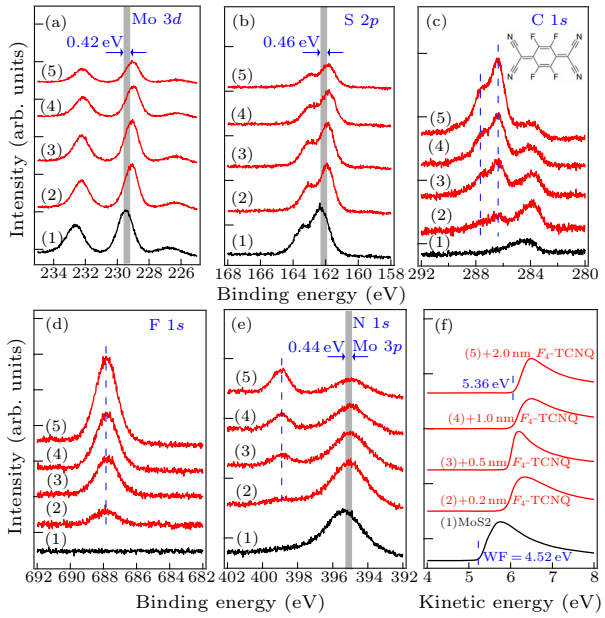

Fig. 3. XPS core level spectra of (a) Mo 3*d*, (b) S 2*p*, (c) C 1*s*, (d) F 1*s*, (e) N 1*s*, and (f) UPS spectra at the low kinetic energy region with the increasing coverage of F_4-TCNQ on bulk MoS_2. The inset of Fig. 3(c) shows the molecular structure of F_4-TCNQ.

Figures 3(a) and 3(b) present the XPS core level spectra of Mo 3*d* and S 2*p* before and after the modification of MoS_2 with F_4-TCNQ. The Mo $3d_{5/2}$ peak shifts to 229.00 eV after the thickness of F_4-TCNQ increases to 2.0 nm, corresponding to a 0.42 eV upward band-bending at the interface. This upward band-bending is also observed in the case of S $2p_{3/2}$ core level, where the S $2p_{3/2}$ peak shows a 0.46 eV shift toward to the low binding energy part. Similar to the case of Cs modified MoS_2, there are no obvious binding energy shifts for the characteristic C 1*s*, F 1*s*, and N 1*s* peaks in F_4-TCNQ, as shown in Figs. 3(c)–3(e). However, the WF of MoS_2 increases from 4.52 eV to 5.36 eV after F_4-TCNQ modification, as illustrated by the significant shift of the secondary electron cut-off toward high kinetic energy part [Fig. 3(f)]. Similar to the case of Cs modified MoS_2, the large vacuum level shift (WF increase) of 0.84 eV derives from the convolution of upward band-bending (0.42 eV) in MoS_2 and the interfacial dipole formed at the F_4-TCNQ/MoS_2 interface [Fig. S2(b)]. The Fermi level of MoS_2 shifts downward due to the electron depletion upon the formation of F_4-TCNQ/MoS_2 interfaces. Moreover, it is worth noting that a 0.44 eV upward binding energy shift of Mo 3*p* core level [Fig. 3(e)] is also observed after the functionalization of MoS_2 by F_4-TCNQ, which further corroborates the p-type doping of MoS_2 by F_4-TCNQ overlayers.

A schematic diagram of energy levels of Cs doped, pristine, and F_4-TCNQ doped MoS_2 is shown in Fig. 4. Charge transfer at the interfaces between dopants and MoS_2 plays a critical role for electrical property tuning of MoS_2. In the case of pristine MoS_2, the Fermi level locates just below the CBM because of the unintentional electron doping deriving from the existence of sulfur vacancies. When low WF Cs has been exploited as surface functionalization overlayers, electron transfer from Cs to MoS_2 occurs, leading to an n-type doping of MoS_2. Meanwhile, when F_4-TCNQ is used to functionalize MoS_2, electron transfer from MoS_2 to F_4-TCNQ occurs because of the strong electron withdrawing property of F_4-TCNQ, leading to a p-type doping of MoS_2.

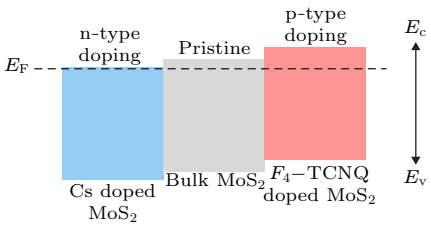

Fig. 4. Schematic diagram of energy levels for Cs doped, pristine, and F_4-TCNQ doped MoS_2.

In summary, tuning the electronic properties of MoS_2 has been realized by Cs and F_4-TCNQ overlayers, which is confirmed by *in situ* UPS and XPS measurements. After the modification of MoS_2 with 2.0 nm Cs, a downward band-bending of MoS_2-related electronic states at the interface has been observed, corresponding to the n-type doping of MoS_2. When 2.0 nm F_4-TCNQ has been deposited onto MoS_2, an upward band-bending of MoS_2-related electronic states has been observed, corresponding to the p-type doping of MoS_2. Our finding indicates that charge transfer at the interfaces between dopants and MoS_2 is of significant importance for the electronic property tuning of MoS_2, and we propose a practical strategy for potential optimization of MoS_2-related electronic and optoelectronic devices.

References

[1] Chhowalla M, Shin H S, Eda G, Li L J, Loh K P and Zhang H 2013 *Nat. Chem.* **5** 263

[2] Wang Q H, Kalantar-Zadeh K, Kis A, Coleman J N and Strano M S 2012 *Nat. Nanotechnol.* **7** 699
[3] Yin Z Y, Li H, Li H, Jiang L, Shi Y M, Sun Y H, Lu G, Zhang Q, Chen X D and Zhang H 2012 *ACS Nano* **6** 74
[4] Cheng R, Jiang S, Chen Y, Liu Y, Weiss N, Cheng H C, Wu H, Huang Y and Duan X F 2014 *Nat. Commun.* **5** 5143
[5] Karunadasa H I, Montalvo E, Sun Y J, Majda M, Long J R and Chang C J 2012 *Science* **335** 698
[6] Lopez-Sanchez O, Lembke D, Kayci M, Radenovic A and Kis A 2013 *Nat. Nanotechnol.* **8** 497
[7] Nagamine Y, Sato J, Qian Y, Inoue T, Nakamura T, Maruyama S, Katsumoto S and Haruyama J 2020 *Appl. Phys. Lett.* **117** 043101
[8] Chen J Y, Liu L, Li C X and Xu J P 2019 *Chin. Phys. Lett.* **36** 037301
[9] Tan C L and Zhang H 2015 *Chem. Soc. Rev.* **44** 2713
[10] Shi W, Zhang X, Li X L, Qiao X F, Wu J B, Zhang J and Tan P H 2016 *Chin. Phys. Lett.* **33** 057801
[11] Zhao Y H, Liu B, Yang J L, He J and Jiang J 2020 *Chin. Phys. Lett.* **37** 088501
[12] Wang H T, Yuan H T, Hong S S, Li Y B and Cui Y 2015 *Chem. Soc. Rev.* **44** 2664
[13] Duan X D, Wang C, Pan A L, Yu R Q and Duan X F 2015 *Chem. Soc. Rev.* **44** 8859
[14] L, Kim H Y, Lotya M, Coleman J N, Kim G T and Duesberg G S 2011 *Adv. Mater.* **23** 4178
[15] Sun D, Huang D, Wang H Y, Xu G L, Zhang X Y, Zhang R, Tang Y G, Abd E H D, Alshitari W, Al-Bogami A S, Amine K and Shao M H 2019 *Nano Energy* **61** 361
[16] Shi Y M, Li H N and Li L J 2015 *Chem. Soc. Rev.* **44** 2744
[17] Wu D, Shi J, Zheng X M, Liu J X, Dou W D, Gao Y L, Yuan X M, Ouyang F P and Huang H 2019 *Phys. Status Solidi R* **13** 1900063
[18] Lin Y C, Zhang W J, Huang J K, Liu K K, Lee Y H, Liang C T, Chu C W and Li L J 2012 *Nanoscale* **4** 6637
[19] Splendiani A, Sun L, Zhang Y B, Li T S, Kim J, Chim C Y, Galli G and Wang F 2010 *Nano Lett.* **10** 1271
[20] Lebègue S and Eriksson O 2009 *Phys. Rev. B* **79** 115409
[21] Mak K F, Lee C, Hone J, Shan J and Heinz T F 2010 *Phys. Rev. Lett.* **105** 136805
[22] Tan S J R, Abdelwahab I, Ding Z J, Zhao X X, YangT S, Loke G Z J, Lin H, Verzhbitskiy I, Poh S M, Xu H, Nai C T, Zhou W, Eda G, Jia B H and Loh K P 2017 *J. Am. Chem. Soc.* **139** 2504
[23] Mouri S, Miyauchi Y and Matsuda K 2013 *Nano Lett.* **13** 5944
[24] Lin J D, Zhong J Q, Zhong S, Li H, Zhang H and Chen W 2013 *Appl. Phys. Lett.* **103** 063109
[25] Wang J W, Ji Z Y, Yang G H, Chuai X C, Liu F J, Z, Lu C Y, Wei W, Shi X W, Niu J B, Wang L, Wang H, Chen J Z, Lu N D, Jiang C, Li L and Liu M 2018 *Adv. Funct. Mater.* **28** 1806244
[26] Park K T and Kong J 2002 *Top. Catal.* **18** 175
[27] Kennou S, Ladas S and Papageorgopoulos C A 1985 *Surf. Sci.* **164** 290
[28] Ladas S, Foulias S D and Papageorgopoulos C A 1984 *Solid State Commun.* **52** 543
[29] Hu P, Ye J, He X X, Du D Z, Zhang K, Wang X Z, Xiong Q H, Liu Z, Jiang H and Kloc C 2016 *Sci. Rep.* **6** 24105
[30] Chen Y Y, Liu F J, Wang J W, Zhang Y, Fan Y, Liu M, Zhao Y F, Wang G T and Jiang C 2020 *Appl. Surf. Sci.* **527** 146709
[31] Chen Z Y, Santoso I, Wang R, Xie L F, Mao H Y, Huang H, Wang Y Z, Gao X Y, Chen Z K, Ma D G, Wee A T S and Chen W 2010 *Appl. Phys. Lett.* **96** 213104
[32] Tsiper E V, Soos Z G, Gao W and Kahn A 2002 *Chem. Phys. Lett.* **360** 47
[33] Stöhr M, Gabriel M and Möller R 2002 *Surf. Sci.* **507** 330
[34] Wüsten J, Ertl T, Lach S and Ziegler C 2005 *Appl. Surf. Sci.* **252** 104
[35] Gu C D, Zhang J L, Sun S, Lian X, Ma Z R, Mao H Y, Guo L, Wang Y P and Chen W 2020 *ACS Appl. Mater. Interfces* **12** 22327

Supplementary Material for "Interfacial Charge Transfer Induced Electronic Property Tuning of MoS_2 by Molecular Functionalization"

SiHan Zhou(周思含)[1], ChunWei Zhou(周春伟)[1], XiangDong Yang(杨向东)[1],

Yang Li(李阳)[1], JianQiang Zhong(钟建强)[*1], HongYing Mao(毛宏颖)[*1]

[1]Department of Physics, Hangzhou Normal University, Hangzhou 311121, China

*Corresponding authors. Email: zhong@hznu.edu.cn (J.Q. Zhong); phymaohy@hznu.edu.cn (H.Y. Mao)

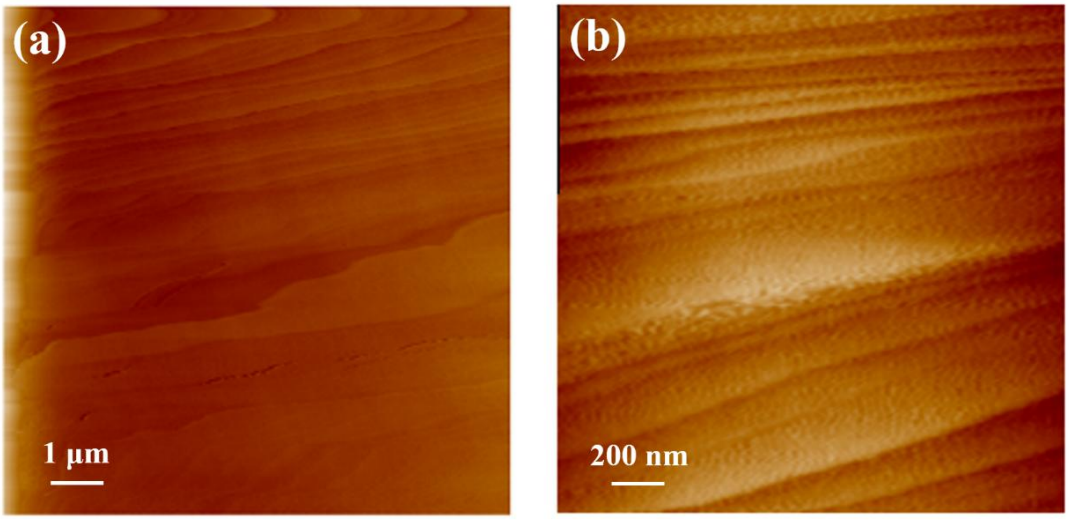

Figure S1 AFM images (10 μm × 10 μm) and (2 μm × 2 μm) of bulk MoS_2.

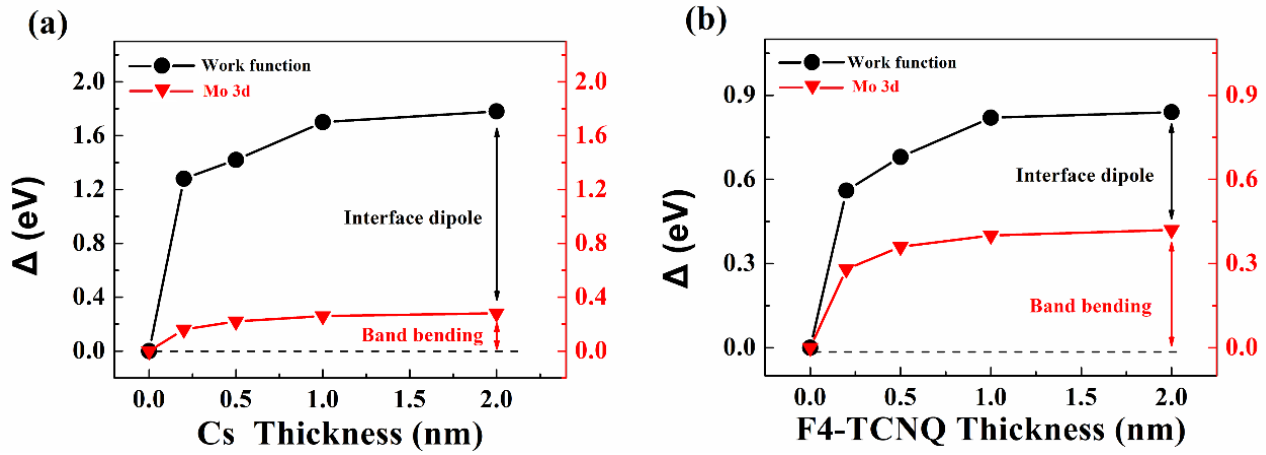

Figure S2 The plot of the sample work function and Mo 3d of MoS_2 as a function of the (a) Cs and (b) F4-TCNQ coverage.

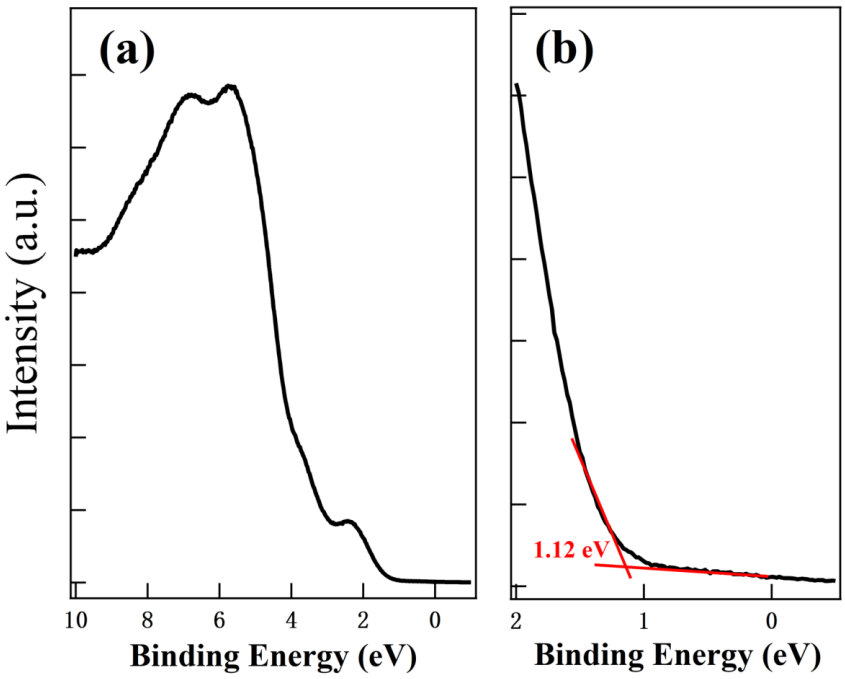

Figure S3 UPS spectrum of bulk MoS2 at (a) the low binding energy part and (b) near the EF region.